ADVANCES IN SCIENCE AND TECHNOLOGY, 43

COMPUTATIONAL MODELING AND SIMULATION OF MATERIALS III

Proceedings of the 3rd International Conference on "Computational Modeling and Simulation of Materials" Acireale, Sicily, Italy, May 30-June 4, 2004, Co-chaired by Jean-Louis Barrat, Tomas Diaz de la Rubia and Masao Doi

PART B

Edited by

P. VINCENZINI
World Academy of Ceramics

A. LAMI
National Research Council, Italy

TECHNA GROUP
Faenza 2004

3rd International Conference
Computational Modeling and Simulation of Materials Part B
P. Vincenzini, A. Lami (Editors) © Techna Group Srl, 2004

Invited Lecture

ABOUT THERMO-SOLUTAL CONVECTION AND GRAIN SEDIMENTATION DURING GLOBULAR EQUIAXED SOLIDIFICATION

A. LUDWIG[1], M. WU[1], T. WANG[2] and A. BÜHRIG-POLACZEK[2]

[1]Department of Metallurgy, University of Leoben, Franz-Josef-Str. 18, A-8700, Leoben, Austria, Tel: +43-(0)3842-402-2201, Fax: +43-(0)3842-402-2202,
Email: ludwig@unileoben.ac.at

[2]Foundry Institute, University of Technology Aachen, Intzestr. 5, D-52072 Aachen, Germany

Based on a two-phase volume averaging model for globular equiaxed solidification a number of important insights on the formation of macrosegregations and on the occurrence of typical grain size distribution pattern in an Al-4wt.% Cu die casting are gained by studying detailed simulation results. The model used considers nucleation and growth of globular equiaxed grains, motion and sedimentation of grains, solute transport by diffusion and convection, and thermo-solutal buoyancy driven flow. Special attention is paid to the impact of thermo-solutal convection and grain sedimentation on the occurrence of macrosegregations and grain size distribution patterns.

1. INTRODUCTION

It is well known that both melt convection as well as motion of grains affect the final microstructure of castings. An example of the affection often occurring in steel ingots is schematically shown in Figure 1. J. Campbell described the complex phenomena occurring with the words[1]: "The interdendritic melt travels towards the roots of the dendrites to feed the solidification shrinkage, the density of the melt tends to rise as a result of falling temperature, but decrease as a result of becoming concentrated in light solute elements such as [C], [S] and [P]. The solutal effects outweigh the thermal effects in this case, the melt tends to rise. Because of its low melting point, the melt tends to dissolve dendrites in its path, and reinforce its channel, as a flooding river carves obstructions from its path. In the same time these channels are responsible for emptying the debris from partially melted dendrites into the bulk melt in the center of the ingot. This fragments fall at a rate somewhere between that of a stone and snow..."

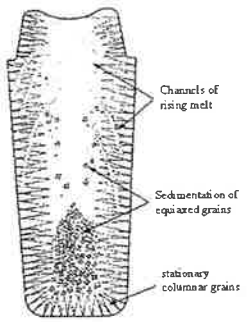

FIGURE 1: Schematic show of the melt convection and grain sedimentation in a steel ingot (taken from Campbell's book[1])

Above description by J. Campbell[1] represents the classical explanation for phenomena occurring during solidification leading to macrosegregations in a conventional steel ingot. The importance of thermo-solutal convection and sedimentation is obvious, not only for steel ingot casting, but for many more industry alloys and processes[2-4].

In the present paper we do not intend to simulate the industry process by including all the physical phenomena occurred during solidification. Rather, we have used a two-phase model developed previously[5-7] to investigate the thermo- and/or solutal convection, grain sedimentation, and their influences on the solidification process and on the formation of macrosegregations in the case of the globular equiaxed solidifying Al - 4.0 wt% Cu alloy. Six different cases with respective model assumptions were simulated: (1) without any convection and sedimentation; (2) with only thermal convection; (3) with only solutal convection; (4) with only grain sedimentation; (5) with combined thermo-solutal convection; and finally (6) with thermo-solutal convection and grain sedimentation. By quantitative studying the role of each individual factor, basic understandings of the phenomena which governs the microstructure formation especially the formation of macrosegregations and the occurrence of typical grain size distribution patterns are gained.

2. BRIEF DESCRIPTION OF THE MODEL

Motion of grains during solidification was first modeled by Beckermann's group based on a volume-averaging approach[8-11]. Beckermann's model was further modified by Ludwig and co-workers for globular equiaxed solidification[5-7]. Details on their approach, which is the basis of the present paper, are described in the original articles. A minor modification compared to the model described in[5-7] is the fact that we have now considered the Boussinesq approximation to model both thermo-solutal convection and gravity-induced grain sedimentation. With $\rho = \rho_s = \rho_l$ the mass conservation equations are given by

$$\frac{\partial}{\partial t}(f_l \rho) + \nabla \cdot (f_l \rho \, \vec{u}_l) = M_{sl} \tag{1}$$

$$\frac{\partial}{\partial t}(f_s \rho) + \nabla \cdot (f_s \rho \, \vec{u}_s) = M_{ls} \tag{2}$$

where f_l and f_s are fraction of liquid and of solid, ρ_l and ρ_s are the densities and $\vec{u}_l$ and $\vec{u}_s$ are the velocities of both phases. $M_{ls}\,(=M_{sl})$ is the mass transfer rate which is defined by the driving force (undercooling), grain number density, grain size, and corresponding growth kinetic parameters[5-7]. The buoyancy forces due to the temperature- and concentration-dependent density and due to the density deference between the free moving grains and the bulk melt are considered only in the source terms ($\vec{F}_l$, $\vec{F}_s$) of the momentum conservation equations (Boussinesq approximation)

$$\frac{\partial}{\partial t}(f_l \rho \, \vec{u}_l) + \nabla \cdot (f_l \rho \, \vec{u}_l \otimes \vec{u}_l) = -f_l \nabla p + \nabla \cdot \bar{\bar{\tau}}_l + \vec{U}_{sl} + \vec{F}_l \tag{3}$$

$$\frac{\partial}{\partial t}\left(f_s \rho\, \vec{u}_s\right)+\nabla\cdot\left(f_s \rho\, \vec{u}_s \otimes \vec{u}_s\right)=-f_s\nabla p+\nabla\cdot\bar{\bar{\tau}}_s+\vec{U}_{ls}+\vec{F}_s \tag{4}$$

Here, $\bar{\bar{\tau}}_l$ and $\bar{\bar{\tau}}_s$ are stress-strain tensors depending on the sheer rate of the flow field and the viscosity of the phases. $\vec{U}_{ls}(=\vec{U}_{sl})$ are momentum exchange terms due to both phase change and drag force. The buoyancy force for the free moving grains is defined as

$$\vec{F}_s = f_s\cdot\rho\cdot\vec{g}_s' \qquad \text{with} \quad \vec{g}_s' = \frac{\Delta\rho}{\rho}\vec{g} = \frac{\rho_s-\rho_l}{\rho}\vec{g} \tag{5}$$

and the thermo-solutal buoyancy force is defined as

$$\vec{F}_l = f_l\cdot\rho\cdot\vec{g}_l' \qquad \text{with} \quad \vec{g}_l' = \frac{\Delta\rho}{\rho}\vec{g} = \frac{\rho_l(T,c)-\rho_l^{ref}}{\rho}\vec{g} \tag{6}$$

$$\text{and} \quad \rho_l(T,c)=\rho_l^{ref}\cdot\left[1+\beta_T\cdot(T^{ref}-T_l)+\beta_c\cdot(c^{ref}-c_l)\right]$$

Other terminologies used in the above equations are explained in Table I. With the Boussinesq approximation the feeding flow due to solidification shrinkage is ignored.

The grain number density, n, is also explicitly solved by means of a grain transport equation[5-7]. A heterogeneous nucleation law[13-14] is implemented as source term in the grain transport equation, and the grains are assumed to be transported with the velocity of the solid phase. With known n and f_s, the average grain size is estimated as

$$d_s = \sqrt[3]{6 f_s/(\pi n)} \tag{7}$$

The liquid and solid concentrations, c_l and c_s, are also explicitly solved by means of a species conservation equations[5-7]. A mixture concentration c_{mix} is used to describe quantitatively the occurrence of macrosegregations.

$$c_{mix} = \frac{c_l\cdot\rho_l\cdot f_l + c_s\cdot\rho_s\cdot f_s}{\rho_l\cdot f_l+\rho_s\cdot f_s} \tag{8}$$

3. PROBLEM DESCRIPTION

In this study we considered the U-shape die casting shown in Figure 2. The casting is assumed to be instantaneously filled with melt of a constant temperature of 925 K. The surrounding mold is kept at a constant temperature of 290 K. The heat transfer coefficient at the casting/mold interface is assumed to be 750 W/m^2/K. A steel chill is intentionally placed at the upper part of the casting to enhance cooling there and so to highlight the effect of grain sedimentation caused by grain nucleation and growth near the chill. The Al - 4.0wt% Cu alloy is selected because of its typical globular equiaxed solidification morphology. The physical parameters used are listed in Table I.

In order to study the impact of melt convection and grain sedimentation on the globular equiaxed solidification process, six different cases with respective modeling assumptions were designed (Table II). Despite of the complexity of the two-phase solidification model, the considered cases still differ from the casting reality. Even in the Case 6 shrinkage flow is ignored. Nevertheless, the comparison of the simulation results of these six cases provide detailed insights to the importance of each individual factor and its role (contribution) to the whole globular equiaxed solidification process.

Table I: Thermophysical and thermodynamic parameters[5, 12]

Thermal conductivity of the melt	k_l	77	W/m/K
Thermal conductivity of the solid	k_s	153	W/m/K
Density of the melt	ρ_l	2606	kg/m
Reference density	ρ^{ref}	2606	kg/m
Reference temperature	T^{ref}	919	K
Reference concentration	c^{ref}	0.04	wt%
Density difference between the solid and the melt	$\Delta\rho$	173	kg/m
Thermal expansion coefficient of the melt	β_T	$1.0\text{x}10^{-4}$	1/K
Solutal (Cu) expansion coefficient of the melt	β_c	$-9.2\text{x}10^{-3}$	1/wt%
Specific heat of the melt	$c_{p(l)}$	1179	J/kg/K
Specific heat of the solid	$c_{p(s)}$	766	J/kg/K
Latent heat of solidification	L	397000	J/kg
Viscosity of the melt	μ_l	$1.2\text{x}10^{-3}$	kg/m/s
Diffusivity of copper in the melt	D_l^{Cu}	$5\text{x}10^{-9}$	m^2/s
Diffusivity of copper in the solid	D_s^{Cu}	$8\text{x}10^{-13}$	m^2/s
Melting point of pure aluminium	T_f	933.5	K
Solute partitioning coefficient	k	0.145	-
Liquidus slope	m	-3.44	K/wt%

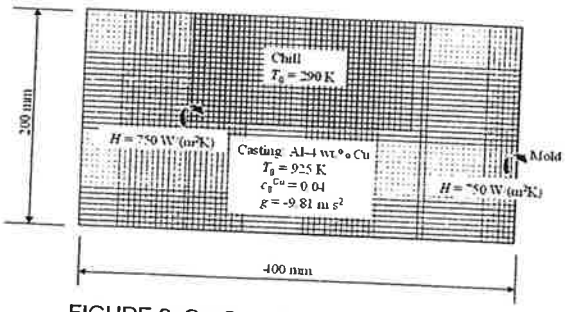

FIGURE 2: Configuration of the benchmark

Table II: Case definition for the simulations

Case 1:	No convection, no grain sedimentation
Case 2:	Thermal convection only
Case 3:	Solutal convection only
Case 4:	Grain movement only
Case 5:	Thermo-solutal convection only
Case 6:	Thermo-solutal convection & grain sedimentation

4. RESULTS AND DISCUSSIONS

4.1. Solidification sequence

The global solidification sequence is described by means of the fraction of solid isolines, $f_s = \text{const.}$. Figure 3 shows f_s-isolines for case 1, 5 and 6.

In case 1, no melt convection and grain sedimentation, the solidification sequence is governed only by heat transfer. It is not surprising that the f_s isolines are identical to the

isotherms (not shown here). Consequently, the last-to-solidify locations, widely called "hot spots", can be predicted by pure heat transfer calculations.

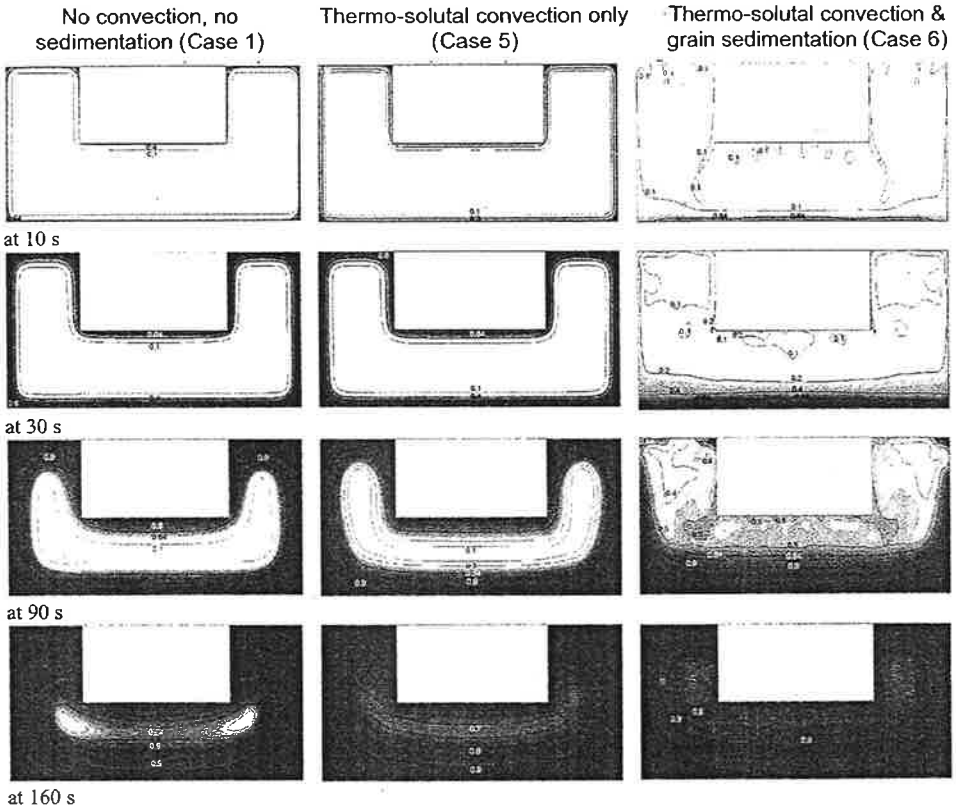

FIGURE 3: Influence of grain sedimentation and melt convection on the global solidificatio sequences. The fraction solid is scaled equidistantly by 30 gray scales from zero (bright) to (black). In addition, f_s-isolines are given.

In case 5, where thermo-solutal convection is considered, the solidification sequence is comparable to case 1 except for the following two differences: (1) the final solidification time for case 5 (estimated to be about 180 seconds) is significant shorter than that of case 1 (about 223 seconds); (2) the predicted "hot spots" in case 5 is shifted slightly upwards compared to case 1. The explanation for the first difference is that the melt convection enhances cooling of the casting: the heat transport through melt convection is faster than that by pure heat conduction. In consequence, the solidification time is reduced. The upward shift of hot spots due to thermo-solutal convection is self-explanatory: the cold and segregated melt (rich in Cu) sinks downwards, and hence the hot and less-segregated melt rises up. The outcome of this kind of convection is to bring heat from lower regions to upper regions.

With both, thermo-solutal convection and grain sedimentation, case 6, the global solidification sequence is no longer predictable by isotherms. The grains in the upper regions, e.g. those nucleated around the chill and also along the side walls, sink downwards. They sedimentate and accumulate in lower bottom region. As the local fraction solid reaches the packing limit (0.637)[5], the solid grains settle there and form a rigid porous body. With this effect, the positions of the hot spots move significantly upwards in comparison to case 1 and case 5. The solidification time of case 6, however, is similar to case 5.

4.2. Thermal against solutal convection

In the following section thermal convection is compared to solutal convection for the Al - 4wt.% Cu U-shape die casting presented in Fig. 2. As the thermal and the solutal expansion coefficients are alloy specific, the outcome of this comparison may differ for other alloys. The influences of thermal convection and of solutal convection on the flow pattern and on the formation of macrosegregations for the considered alloy and geometry is shown in Figure 4.

As expressed in Eq. (6), the driving forces for thermal and solutal convection are the terms $\beta_T \cdot \left(T^{ref} - T_l\right)$ and $\beta_c \cdot \left(c^{ref} - c_l\right)$. For Al - 4wt.% Cu the thermal expansion coefficient β_T is positive: the colder melt has the higher density, and thus tends to sink downwards. In opposite, the solutal expansion coefficient β_c is negative for the considered alloy: melt rich in solute (Cu) is denser, and thus tends to sink as well. In the considered casting the temperature gradient from the mold walls towards the casting center is always positive, leading to a downwards motion of melt near the walls, even if solidification occurs. The same downwards motion of melt is caused by the fact that melt from partly solidified regions reveals a higher concentration (for Al - 4wt.% Cu yields $k < 1$). Thus, the melt near the mold walls has higher density due to both thermal and solutal reasons. Therefore, similar flow patterns are observed for both cases. However, the maximal velocity in case 3 (solutal convection) is much higher than that of case 2 (thermal convection): after 70 seconds the maximal velocity in case 3 is 2.45 mm/s compared to only 0.1 mm/s in case 2. From the simulated temperature and concentration field, it can be shown that at 70 seconds the temperature difference between the bulk melt and the melt near the side wall is about 100 K, while the concentration difference between the bulk melt and the melt near the mold wall is about 16 wt.%. This lead to a driving force for thermal convection, $\beta_T \cdot \left(T^{ref} - T_l\right)$, in the order of 10^{-2}, and for solutal convection in the order of 10^{-1}. Consequently, solutal convection is the dominating mechanism compared to the thermal one and the predicted macrosegregation in case 3 is stronger than in case 2.

Note that in both cases the downwards motion of melt along the vertical walls leads to the occurrence of two vortexes in each half of the casting: for the left half this is an anti-clockwise vortex near the outer wall and a clockwise vortex near the chill wall. As the process proceed the vortex caused from the downwards motion of melt near the outer wall becomes dominant and the other disappeared (compare 70 and 130 seconds at Fig. 4), so that only one vortex in each half of the casting prevail.

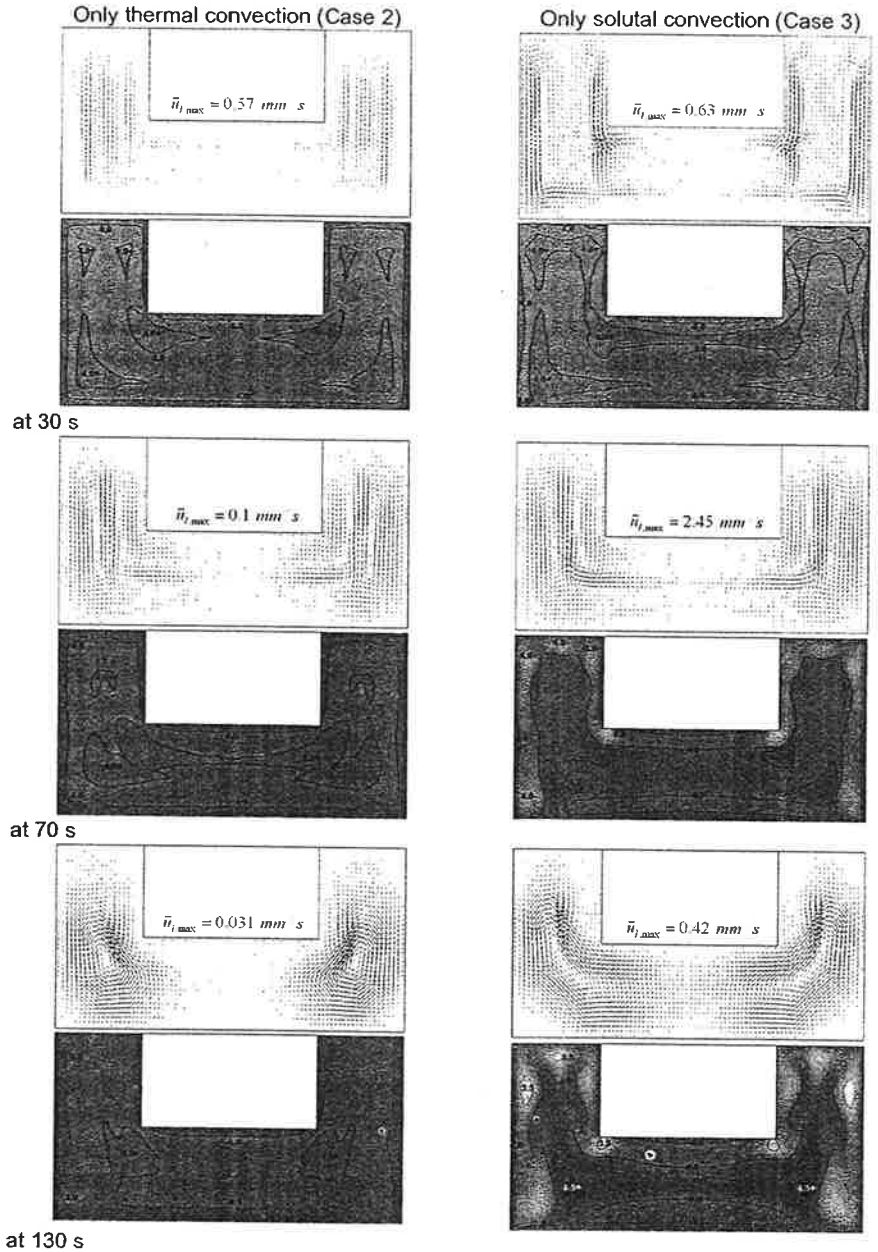

FIGURE 4: Comparison of thermal and solutal convection, and their influences on macrosegregation. The mixture concentration c_{mix} is scaled equidistantly by 30 gray scales from 3 wt% (bright) to 5 wt% (dark). The arrows of the melt velocity are continuously scaled from zero to the given maximum value.

In both cases macrosegregations form due to the relative motion between flowing melt and non-moving solid. As the melt flow is much stronger in case 3 the occurrence of macrosegregations is much more pronounced if solutal convection is considered. Generally, the melt flow carries segregated melt from semi-solid regions (mushy zone) into regions without any (or with less) solid. This convective solute transport causes negative segregated areas to occur in semi-solid regions and positive segregated areas to occur in the bulk melt (or at the boundary of the mushy zone). In the present cases positive segregations (areas in Figure 4 darker than the average) are built up gradually near areas with low solid fraction at beginning of solidification, e.g. at 30 second. These positive segregation areas move as the melt flow. With proceeding solidification, more solute elements are further brought into these already segregated regions, and the positive segregations become stronger and wider. In the late stage of solidification, e.g. at 130 second, different positive segregation areas joint together, forming larger and stronger segregation zones in the last-to-solidify regions. Opposite to the positive segregated areas, the negative segregated ones (in Figure 4 lighter than the average) do not move. They are associated with areas of large solid fraction, where the corresponding segregated melt had been washed away and replaced by less segregated melt. While solidification proceed also these negative segregated areas become larger and more pronounced.

4.3. Macrosegregation during equiaxed solidification

The formation of macrosegregations in case 6, where both thermo-solutal convection and grain sedimentation is counted for, is more complicated than in case 2 or 3. In previous publications by the authors[5-7] same insights in the different formation mechanisms are given.

Corresponding conclusions can be summarized as follows: (1) grain settlement results in negative segregation; (2) depletion (leaving) of grains from a volume element, and the corresponding feed-in with segregated melt to replace the space of leaving grains will cause positive segregation in this volume element; (3) squeezing out of the segregated melt by settling grains will cause positive segregation near the settlement region; (4) in regions with high solid fraction where the packing limit is exceeded, feeding with segregated melt leads to positive segregation, feeding with less-segregated melt leads to negative segregation. The macrosegregation shown in Figure 5 can be explained by the first three of these mechanisms.

Negative segregations in the bottom regions, especially near both side walls, are mainly caused by mechanism (1), namely grain settlement. These negative segregation zones will stay where they form. They become wider as solidification and settlement continue, but generally they do not move. The positive segregated areas, forming just above (or nearby) the settlement zones are due to mechanism (3), namely squeezing out of segregated melt by settling grains. Obviously these positive segregated areas, locate originally at the boundary of the two-phase zone move with the melt flow current: they spread out following the flow lines of the melt. While solidification proceeds, these positive segregated areas move towards and accumulate in the last-to-solidify regions, forming a large positive center segregation. Mechanism (4) (not accounted for in this

paper) works only in dense packed zones where the solid cannot move anymore. However, its impact on chances in strength and size of segregated areas is of minor importance compared with the other mechanisms mentioned above.

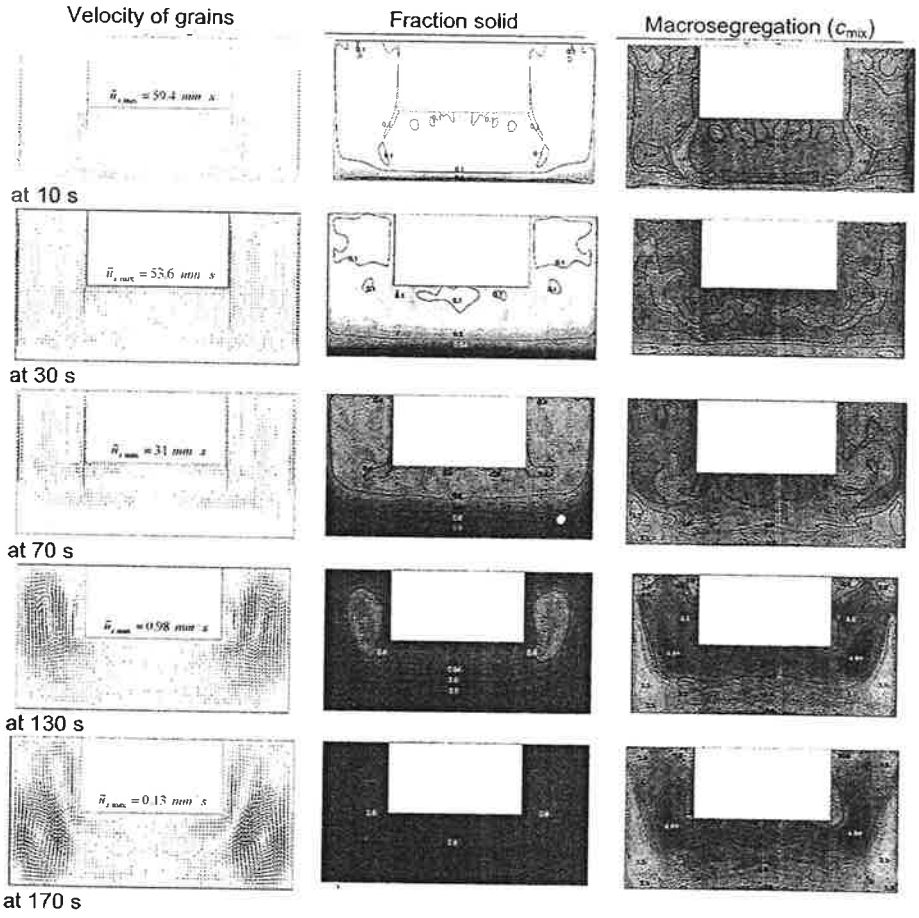

FIGURE 5: Macrosegregation formation in globular equiaxed solidification. The mixture concentration is scaled equidistantly by 30 gray scales from 2.5 wt% (bright) to 5.5 wt% (dark), while the fraction solid is scaled from zero (bright) to 0.999 (dark). The arrows of the melt velocity are continuously scaled from zero to the given maximum value.

4.4. Grain size distribution

The appearance of a certain grain size distribution pattern is the joint result of nucleation, growth kinetics, melt convection and grain sedimentation. In Figure 6 the formation of the grain size distribution for case 1 (no melt convection or grain sedimentation) is compared with case 6 (with both melt convection and grain sedimentation). Note that the final grain size distribution pattern is completely different. In

case 1 a certain pattern with grain sizes ranging from 120 µm in the corners up to over 200 µm in a band around the chill is predicted. In opposite to that, the grain size distribution calculated for case 6 is much more uniform with grain sizes ranging from 140 µm to slightly above 160 µm.

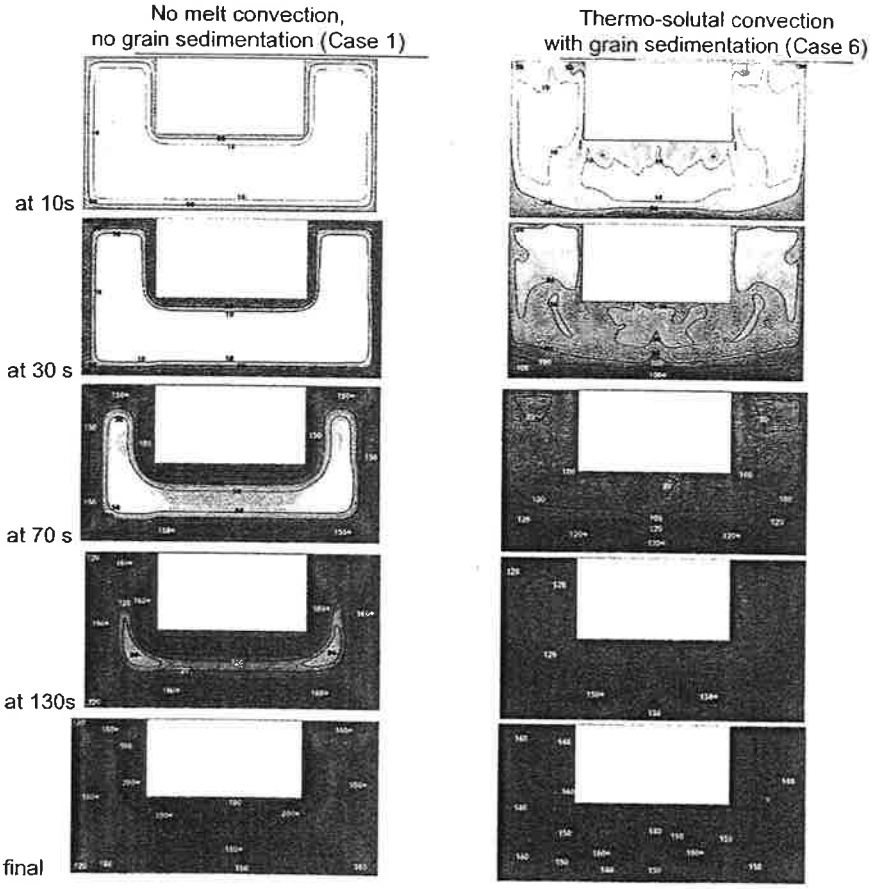

FIGURE 6: Grain size evaluation. The grain size is scaled equidistantly by 30 gray scales from zero (bright) to 234 µm (dark) for case 1, while from zero (bright) to 165 µm (dark) for case 6.

We have investigated the origin of the pattern occurring in case 1 and found that it is mainly caused by a similar pattern in the number density of grains. The number density of grains on the other hand is an accumulated result of the nucleation events occurring, which itself is governed by the local undercooling. As high undercooling is enhanced by larger cooling rates, the number density pattern, and so the grain size distribution pattern, reflects somehow the heat extraction history.

Although in real castings no melt convection and no grain sedimentation (case 1) are somehow insufficient assumptions, it is interesting to compare the grain size distribution

pattern calculated for case 1 with existing classical approaches. A well-known empirical relationship[3] between dendrite arm spacing λ and cooling rate $\dot{T}$ is

$$\lambda = b \cdot \left(\dot{T}\right)^{-n} \tag{9}$$

with constant b and exponent n ranging between 1/3 to 1/2 for secondary spacing and generally very close to 1/2 for primary spacing. Further on, it is often assumed that the size of equiaxed grains is comparable to the primary dendrite arm spacings. Therefore, we calculated the distribution of the criterion function $1/\sqrt{\dot{T}}$ (assuming n = 1/2) for the U-shape die casting considered in this work. Figure 7 show, that the $1/\sqrt{\dot{T}}$ distribution coincides remarkable well with the predicted grain size distribution for case 1. Although both the empirical relationship and case 1 assume heat transport by conduction only, it is somehow exciting that an empirical relationship which is based on a solidification model gives results comparable to a model based on nucleation. On the other hand, disregarding melt convection and grain sedimentation makes the prediction of grain size distribution appearing in real casting unrealistic as the impact of melt convection and particularly that of grain sedimentation on the final size distribution is large (Figure 6).

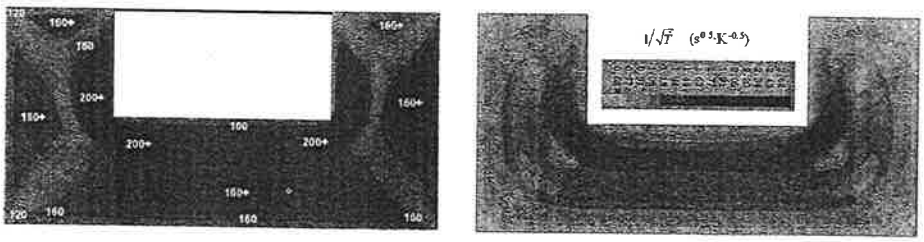

FIGURE 7: left: grain size distribution for case 1, right: distribution of $1/\sqrt{\dot{T}}$ numerically calculated considering heat transfer only. The similarity of the pattern is obvious (and clearer visible in color).

5. CONCLUSIONS

The numerical investigations presented in this paper can be gathered in the following conclusions:

1. In globular equiaxed solidification, the proceeding of solidification can not be simply predicted with isotherms. The impact of grain sedimentation and thermo-solutal convection on the solidification process shifts the final solidification spots significantly upwards.
2. For the Al - 4.0wt% Cu alloy the influence of solutal convection on the formation of macrosegregations overweigh that of thermal convection. However, when grain sedimentation is considered, both the strength and the distribution of the macrosegregations is quite different. Grain sedimentation leads to large negative segregation zones in the bottom regions of the casting. Large positive segregation zones are predicted in the last-to-solidify regions.

3. Final grain size distribution in globular equiaxed solidification is the joint result of nucleation, growth kinetics, melt convection and grain sedimentation. An exciting finding is that if melt convection and grain sedimentation is ignored the predicted grain size distribution is comparable with the empirical relationship $d \propto 1/\sqrt{\dot{\varepsilon}}$. On the other hand, by considering melt convection and particularly grain sedimentation the predicted size distribution is much more uniform and the above empirical relationship is no more suitable for the prediction of grain sizes.

ACKNOWLEDEMENT

The authors acknowledge the excellent technical assistance of Dr. Pelzer with FLUENT Germany. AL and MW also acknowledge the financial support by the Christian-Doppler Society within the frame of the CD-laboratory "Multiphase Modelling of Metallurgical Processes".

REFERENCES

[1] J. Campbell, *Castings*, (Oxford: Butterworth-Heinemann Ltd, 1991)
[2] A.Ohno, *Solidification-The Separation Theory and its Practical Applications*, (Berlin: Springer-Verlag, 1987)
[3] M.C. Flemings, *Solidification Processing*, (New York, NY: McGrow-Hill, Inc., 1974)
[4] C. Beckermann, *Intern. Mater. Rev.*, Vol 47, 2002, pp. 243-261.
[5] A. Ludwig, M. Wu, Metall. *Mater. Trans.* Vol 33A, 2002, pp. 3673.
[6] M. Wu, A. Ludwig, *Adv. Eng. Mater.*, vol. 5, 2003, pp. 62
[7] M. Wu, A. Ludwig, A. Bührig-Polaczek, M. Fehlbier, P.R. Sahm, *Int. J. Heat Mass Transfer.*, Vol 46, 2003, pp. 2819-2832
[8] J. Ni, C. Beckermann, *Metall. Trans.*, Vol 22B, 1991, pp. 349
[9] C. Beckermann and R. Viskanta, *Appl. Mech. Rev.* Vol 46, No. 1, 1993, pp.1
[10] C.Y. Wang, C. Beckermann, *Metall. Mater. Trans.*, Vol 27A, 1996, pp. 2754
[11] C. Beckermann, *Intern. Mater. Rev.*, Vol 47, 2002, pp. 243
[12] R. Trivedi, S. Liu, P. Mazumder, E. Simsek, *Sci. Techn. Adv. Mater.*, Vol 2, 2001, pp.309-320.
[13] W. Oldfield, *Trans. ASM*, Vol. 59, 1966, pp. 945-961.
[14] M. Rappaz, *Int. Mater. Rev.*, Vol. 34, 1989, pp. 93-123.